Journal of Inorganic Biochemistry 104 (2010) 467–476

Contents lists available at ScienceDirect

Journal of Inorganic Biochemistry

journal homepage: www.elsevier.com/locate/jinorgbio

Zinc(II) complexes of 2-acetyl pyridine 1-(4-fluorophenyl)-piperazinyl thiosemicarbazone: Synthesis, spectroscopic study and crystal structures – Potential anticancer drugs

Tatjana P. Stanojkovic [b], Dimitra Kovala-Demertzi [a,*], Alexandra Primikyri [a], Isabel Garcia-Santos [c], Alfonso Castineiras [c], Zorica Juranic [b], Mavroudis A. Demertzis [a]

[a] Inorganic and Analytical Chemistry, Department of Chemistry, University of Ioannina, 45100 Ioannina, Greece
[b] Institute for Oncology and Radiology of Serbia, Pasterova 14, 11000 Belgrade, Serbia
[c] Departamento de Química Inorgánica, Universidad de Santiago de Compostela, E-15706 Santiago de Compostela, Spain

ARTICLE INFO

Article history:
Received 11 June 2009
Received in revised form 30 December 2009
Accepted 31 December 2009
Available online 7 January 2010

Keywords:
Zn(II)
Complexes
Thiosemicarbazone
Crystal structure
In vitro antitumor activity
Biological evaluation

ABSTRACT

2-Acetyl pyridine thiosemicarbazone containing an 1-(4-fluorophenyl)-piperazinyl ring incorporated at N(4)-position, HAcPipPheF (**1**) and the zinc(II) complexes $[Zn(AcPipPheF)_2]$ (2) and $[Zn(OAc)(AcPipPheF)]_2$ (**3**) have been prepared and structurally characterized by means of vibrational and NMR (^1H and ^{13}C) spectroscopy. The crystal structures of the compounds **1**–**3** have been determined by X-ray crystallography. The metal coordination geometry of $[Zn(AcPipPheF)_2]$ is described as distorted octahedral configuration in a *trans*-N–*cis*-N–*cis*-S configuration. In $[Zn(OAc)(AcPipPheF)]_2$ one of the acetato group exhibits monoatomic bridge and the other bridges in a bidentate manner. The zinc(1) metal ion is coordinated in a distorted octahedral configuration while the metal coordination of Zn(2) is described as distorted square pyramidal. Biomedical studies revealed that, compounds **1**–**3** displayed potent anticancer activity. The antiproliferative activity of **1**–**3** was found to be considerably stronger than that of *cis*-platin. The IC_{50} values range from 26 to 90 nM, against all cell lines tested, while for *cis*-platin the IC_{50} values range from 2 to 17 μM and for the zinc salt, $ZnCl_2$, the IC_{50} values range from 81 to 93 μM. The complex **3** shows the highest activity against all four cancer cell lines and the highest selectivity against K562 and MDA-MB-453 cancer cell lines. The compounds inhibited tumor cell proliferation by arresting the cell cycle progression at the S phase.

1. Introduction

Thiosemicarbazones are versatile molecules not only because of their broad profile in pharmacological activity, but also because can act as ligands in coordination chemistry in different ways. It has been demonstrated in previous publications that thiosemicarbazones afford a diverse variety of compounds with different activities [1–7]. The mechanism of action of TSCs, is due to its ability to inhibit the biosynthesis of DNA, possibly blocking the enzyme ribonucleotide diphosphate reductase; binding to the nitrogen bases of DNA or RNA, hindering or blocking base replication; creation of lesions in DNA strands by oxidative rupture [1].

Zinc the second most prominent trace metal in the human body after iron is essential for growth, development and plays an important role in various biological systems. It is a vital component an essential cofactor, critical for numerous cellular processes and may be a major regulatory ion in the metabolism of cells. Zinc is cytoprotective and suppresses apoptotic pathways. Zinc plays a role in brain, where it has a specific function as a neuromodulator in addition to its other typical cellular functions [7,8]. A structural review of main group metal complexes of semicarbazones and thiosemicarbazones shows that TSCs are very versatile coordination agents with these acceptors [9].

Given the potential biological activity of thiosemicarbazones and the involvement of the Zn(II) in the metabolism of cells and our previous results on Zn(II) TSCs complexes [10–12], we thought it would be of interest to explore this chemistry. In order to widen the scope of investigations on the coordination behaviour of TSCs, towards Zn(II), we carried out systematic studies with the final goal to develop new biologically active pharmaceuticals. With metallopharmaceuticals playing a significant role in therapeutic and diagnostic medicine, the discovery and development of new metallodrugs remain an ever-growing area of research in medicinal inorganic chemistry.

The present paper includes synthesis, spectral characterization of the novel prepared zinc(II) complexes with 2-acetylpyridine N(4)-(4-fluorophenyl)-piperazine thiosemicarbazone, HAcPipPheF,

* Corresponding author. Tel.: +30 2651098425; fax: +30 2651098791.
E-mail address: dkovala@cc.uoi.gr (D. Kovala-Demertzi).

0162-0134/$ - see front matter © 2010 Elsevier Inc. All rights reserved.
doi:10.1016/j.jinorgbio.2009.12.021

1 (Scheme 1) and the crystal structure of the ligand and the complexes [Zn(AcPipPheF)$_2$] (**2**) and [Zn(OAc)(AcPipPheF)]$_2$ (**3**). The compounds **1–3** were tested for their antiproliferative activity *in vitro* against the cells of four human cancer cell lines: HeLa (cervix adenocarcinoma cell line), K562 (chronic myelogenous leukaemia), MDA-MB-361 and MDA-MB-453 (breast cancer cell lines).

2. Experimental

2.1. General and instrumental

All reagents were commercially available (*Aldrich* or Merck) and used as supplied. Solvents were purified according to standard procedures. The MTT (3-(4,5-di-methyl-thiazol-2-yl)-2,5-diphenyl tetrazolium bromide) was dissolved (5 mg/mL) in phosphate buffer saline pH 7.2 and filtered (0.22 μm) before use. The RPMI-1640 cell culture medium, fetal calf serum, MTT, ethidium bromide and acridine orange were purchased from Sigma Chemical Company, USA. Melting points were determined in open capillaries and are uncorrected. Infrared and far-infrared spectra were recorded on a Perkin Elmer Spectrum GX Fourier transform spectrophotometer using KBr pellets (4000–400 cm^{-1}) and Nujol mulls dispersed between polyethylene disks (400–40 cm^{-1}). The intensity of reported IR signals is defined as m = medium, mw = medium weak, s = strong, ms = medium strong. NMR spectra were recorded on a Bruker AV-400 spectrometer operating at 400 and 100 MHz for ^{1}H and ^{13}C acquisition, respectively, or on a Bruker AV-250 spectrometer operating at 250.13 and 62.90 MHz for ^{1}H and ^{13}C acquisition respectively. The splitting of proton resonances in the reported ^{1}H NMR spectra is defined as s = singlet, d = doublet, t = triplet, and m = multiplet. The spectra were acquired at room temperature (298 K). The chemical shifts are reported in ppm for ^{1}H and ^{13}C NMR. Samples were dissolved in dimethylsulfoxide-d$_6$ and spectra were obtained at room temperature with the signal of free dimethylsulfoxide-d$_6$ (at 2.50 ppm ^{1}H NMR, 39.5 ppm ^{13}C NMR) as a reference. Mass spectra were recorded on an Agilent LC/MSD Trap SL spectrometer. Elemental analyses, C, H, N and S were performed on a Carlo Erba EA (model 1108).

2.2. Synthesis of the ligand and the complexes

2.2.1. Preparation of 2-acetylpyridine-N4-1-(4-fluorophenyl)piperazinyl thiosemicarbazone, HAcPipPheF; (*1*)

4-Methyl-4-phenyl-3-thiosemicarbazide was prepared according to the method described by Scovill et al. [13]. The crude product, 4-methyl-4-phenyl-3-thiosemicarbazide, was recrystallized from a mixture of EtOH and distilled water (3:1). 1-(4-fluorophenyl)-piperazine (0.5407 g, 3 mM) and 2-acetylpyridine (0.363 mL, 3 mM) were added to a solution of 4-methyl-4-phenyl-3-thiosemicarbazide (0.543 g, 3 mM) in CH_3CN (4 mL). The mixture was stirred and refluxed for 30 min. The resulting yellow precipitate was filtered off, washed with cold CH_3CN and dried *in vacuo* over silica gel. M.p. 155–157 °C. Yield: 56%. IR (cm^{-1}): 3218m, *ν*(NH); 2838m, *ν*(CH); 1584mw, *δ*(NH); 1561m, 1512s, *ν*(C=C) *ν*(C=N); 1416s, 1363s, 1297s, *ν*(NCS); 1223s, (Ar–F); 1088m, *ν*(N–N); 931s, *ν*(CS); 650m, *δ*(py). ^{1}H NMR (DMSO-d$_6$) *δ* (ppm): 9.35 (s, 1H, N(3)H); 8.71 (d, 1H, *J* = 4.4 Hz, C(1)H); 7.49 (t, 1H, *J* = 5.7 Hz, C(2)H); 7.92–7.95 (m, 1H, C(3)H); 7.95–7.97 (m, 1H, C(4)H); 2.57 (s, 3H, C(7)H); 4.14 (t, 4H, C(9,11)H); 3.19 (t, 4H, C(10,12)H); 6.98–7.04 (m, 2H C(14,18)H); 7.05–7.13 (m, 2H, C(15,17)H); ^{13}C NMR *δ* (ppm): 150.25 C(1); 125.71 C(2); 138.48 C(3); 122.34 C(4); 155.28 C(5); 148.48 C(6); 14.10 C(7); 184.37 C(8); 50.02 C(9,11); 49.61 C(10); 48.03 C(12); 148.51 C(13); 118.35 C(14); 116.12 C(15); 159.04 C(16); 116.47 C(17); 118.47 C(18); Mass spectrum, MS (electrospray Ionization, ESI, *m*/*z*): 358 [**1**+H]$^+$, 380 [**1**+Na]$^+$, 326 [**1**−S]$^+$. Elemental analysis are consistent with $C_{18}H_{20}N_5SF$ found: C, 60.3; H, 5.6; N, 19,3; S, 8.9; Calc.: C, 60.5; H, 5.5; N, 19.6; S, 9.0. Suitable crystals for X-ray study were obtained by crystallization from a fresh solution of $CHCl_3/C_6H_6$.

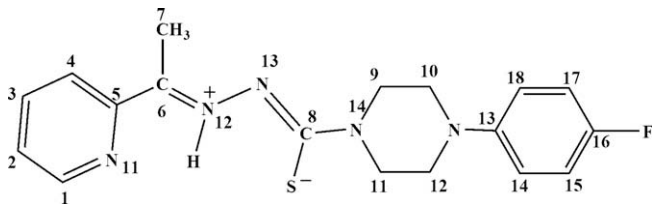

Scheme 1. The numbering scheme for HAcPipPheF, **1**, showing the positively charge N12 and the negatively charged S.

2.2.2. Preparation of bis(2-acetylpyridine-N4-1-(4-fluorophenyl)-piperazinyl thiosemicarbazonato)zinc(II), [Zn(AcPipPheF)$_2$]; (*2*)

A solution of $ZnCl_2$ (0.068 g, 0.5 mM) in 10 mL of EtOH was added to a solution of HAcPipPheF (0.393 g, 1.1 mM) in 15 mL of EtOH. The mixture was stirred and some drops of Et_3N were added. The apparent pH value was 8. The solution was refluxed for 2 h in 80 °C and was left in the fridge overnight. The yellow precipitate was filtered off, washed with cold EtOH and dried *in vacuo* over silica gel. M.p. 275–277 °C. Yield: 48.0%. IR (cm^{-1}): 2828s, *ν*(CH); 1591s, 1548w, 1507s, *ν*(C=C) *ν*(C=N); 1417s, 1366s, 1299s, *ν*(NCS); 1220s, *ν*(Ar–F); 1155s, *ν*(N–N); 928s, 869m, *ν*(CS); 662w, *δ*(py); 433m, 419m, *ν*(Zn–N); 382m, 369m, *ν*(Zn–S); 255m, 239m, *ν*(Zn–N$_{pyr}$) cm^{-1}. ^{1}H NMR (DMSO-d$_6$) *δ* (ppm): 8.65 (d, 1H, C(1)H); 7.33 (t, 1H, *J* = 6.2 Hz, C(2)H); 7.84 (t, 1H, *J* = 4.5 Hz, C(3)H); 7.94 (t, 1H, *J* = 7.5 Hz, C(4)H); 2.66 (s, 3H, C(7)H); 4.10 (t, 4H, C(9,11)H); 3.16 (t, 4H, C(10,12)H); 7.02–7.08 (m, 2H, C(14,18)H); 7.10–7.14 (m, 2H, C(15,17)H); ^{13}C NMR *δ* (ppm): 150.63 C(1); 124.65 C(2); 139.66 C(3); 121.99 C(4); 154.90 C(5); 146.01 C(6); 14.12 C(7); 181.43 C(8); 49.81 C(9,11); 46.85 C(10,12); 148.51 C(13); 118.13 C(14); 116.07 C(15); 158.62 C(16); 115.72 C(17); 118.01 C(18). MS (ESI, *m*/*z*): 779 [**2**+H]$^+$. Elemental analysis are consistent with $ZnC_{36}H_{38}N_{10}S_2F_2$ found: C, 55.3; H, 5.1; N, 17.8; S, 8.0; Zn, 8.10. Calc.: C, 55.6; H, 4.9; N, 18.0; S, 8.2; Zn, 8.40. Suitable crystals for X-ray study were obtained by crystallization from a fresh solution of $EtOH/C_6H_6$.

2.2.3. Preparation of bis(μ-acetato(2-acetylpyridine-N4-1-(4-fluorophenyl)-piperazinyl thiosemicarbazonato)zinc(II), [Zn(HAcPipPheF)(OAc)]; (*3*)

A solution of [Zn(CH$_3$COO)$_2$(H$_2$O)$_2$] (0.241 g, 1.1 mM) in 10 mL of EtOH was added to a solution of HAcPipPheF (0.357 g, 1 mM) in 15 mL of EtOH. The mixture was stirred and some drops of Et_3N were added. The apparent pH value was 8. The solution was refluxed for 2 h and then it was left in the fridge overnight. The yellow precipitate was filtered off, washed with cold EtOH and dried in vacuo over silica gel. Yield: 77.3%. M.p. 280–282 °C. IR (cm^{-1}): 2812s, *ν*(CH); 1580s, 1506s, *ν*(C=C) *ν*(C=N); 1412s, 1366s, 1299s *ν*(NCS); 1217s, *ν*(Ar–F); 1152s, *ν*(N–N); 816s, *ν*(CS); 1655s, 1590s ν_{as}(COO); 1367ms, 1455s, ν_s(COO); 665mw, *δ*(py); 427ms, *ν*(Zn–N); 372ms, *ν*(Zn–S); 250ms, *ν*(Zn–N$_{pyr}$), 376ms, 346ms, 328ms, *ν*(Zn–O) cm^{-1}. ^{1}H NMR (DMSO-d$_6$) *δ* (ppm): 8.49 (d, 1H, *J* = 4.3 Hz, C(1)H); 7.58 (t, 1H, *J* = 6 Hz, C(2)H); 7.86 (t, 1H, *J* = 8.5 Hz, C(3)H); 8.11 (t, 1H, *J* = 7.8 Hz, C(4)H); 2.66 (s, 1H, C(7)H); 4.11 (t, 4H, *J* = 3.7 Hz, C(9,11)H); 3.17 (t, 4H, *J* = 5 Hz, C(10,12)H); 7.04–7.08 (m, 2H, C(14,18)H); 7.10–7.11 (m, 2H, C(15,17)H); 1.79 (s, 3H, OAc); ^{13}C NMR *δ* (ppm): 150.76 C(1); 125.48 C(2); 141.06 C(3); 122.45 C(4); 155.27 C(5); 145.82 C(6); 14.07 C(7); 180.73 C(8); 50.13 C(9,11); 47.09 C(10,12); 148.80 C(13); 118.42 C(14); 116.44 C(15); 158.50 C(16); 116.09 C(17); 118.54 C(18); 23.96, 176.50 CH_3COO^-; MS (ESI, *m*/*z*): 960 [**3**+H]$^+$.

Elemental analysis are consistent with $ZnC_{20}H_{22}N_5SFO_2$ found: C, 49.7; H, 4.9; N, 14.1; S, 6.5; Zn, 13.45. Calc.: C, 50.0; H, 4.6; N, 14.6; S, 6.7; Zn, 13.60. Suitable crystals for X-ray study were obtained by crystallization from a fresh solution of $CHCl_3$/THF (where THF is tetrahydrofurane).

2.3. X-ray crystallography

Crystal data and experimental details are listed in Table 1. A yellow prismatic crystal of **1** and yellow plate crystals of **2** and **3** were mounted on a glass fiber and used for data collection. Crystal data were collected at 100.0(1) K, using a Bruker X8 KappaAPEXII diffractometer. Graphite monochromated Mo K(alpha) radiation (lambda = 0.71073 Å) was used throughout. The data were processed with APEX2 [14] and corrected for absorption using SADABS (transmissions factors: 1.000–0.936, 1.000–0.766 and 1.000–0.873) for **1, 2** and **3**, respectively [15]. The structure was solved by direct methods using the program SHELXS-97 [16] and refined by full-matrix least-squares techniques against F^2 using SHELXL-97 [17]. Positional and anisotropic atomic displacement parameters were refined for all non-hydrogen atoms. Hydrogen atoms were located in difference maps and included as fixed contributions riding on attached atoms with isotropic thermal parameters 1.2 times those of their carrier atoms. Criteria of a satisfactory complete analysis were the ratios of "rms" shift to standard deviation less than 0.001 and no significant features in final difference maps. Atomic scattering factors from "International Tables for Crystallography" [18] and molecular graphics from PLATON [19].

2.4. Biological experiments

2.4.1. Antiproliferative assay in vitro

2.4.1.1. Compounds. Stock solutions of investigated compounds, were prepared in DMSO at concentrations of 10 mM and afterwards they were diluted with complete nutrient medium (RPMI-1640 without phenol red) supplemented with 3 mM L-glutamine, 100 μg/mL streptomycin, 100 IU/mL penicillin, 10% heat inactivated fetal bovine serum (FBS), and 25 mM: 2-[4-(2-hydroxyethyl)1-piperazino]ethanosulfonosäure (Hepes) adjusted to pH 7.2 by bicarbonate solution. RPMI-1640, FBS, Hepes, and L-glutamine were products of Sigma Chemical Co., St. Louis, MO. The final concentrations of the compounds were 50, 10, 1, 0.1, and 0.01 μM.

2.4.1.2. Tumor cell lines. Human cervix adenocarcinoma HeLa cells, human chronic myelogenous leukaemia K562, human breast cancer MDA-MB-361 and MDA-MB-453 cells were cultured as a monolayer, while were grown in a suspension in the complete nutrient medium, at 37 °C in humidified air atmosphere with 5% CO_2. For the growth of MDA-MB-361 and MDA-MB-453 cells complete medium was enriched with 1.11 g/L glucose. Neoplastic HeLa cells (2000 cells per well), MDA-MB-361 cells (7000 cells per well), MDA-MB-453 cells (3000 cells per well), were seeded into 96-well microtiter plates. Twenty-four hours later, after the cell adherence, five different, double diluted, concentrations of investigated compounds were added to the wells, except for the control cells to which a nutrient medium only was added. K562 cells (3000 cells per well) were seeded, 2 h before addition of investigated compounds to give the desired final concentrations. Nutrient medium was RPMI-1640, supplemented with L-glutamine (3 mM), streptomycin (100 lg/mL), and penicillin (100 IU/mL), 10% heat inactivated (56 °C) FBS and 25 mM Hepes, and the pH of the medium was adjusted to 7.2 by bicarbonate solution. The cultures were incubated for 72 h.

2.4.1.3. MTT test. Cell survival was determined by MTT test [20,21] 72 h upon addition of the compounds. Briefly, 20 μL of MTT solution (3-(4,5-dimethylthiazol-2-yl)-2,5-diphenyltetrazolium bromide, 5 mg/mL in phosphate buffered saline) was added to each well. Samples were incubated for further four h. Then, 100 μL of 10% SDS was added to extract the insoluble product formazan, resulting from the conversion of the MTT dye by viable cells. The number of viable cells in each well was proportional to the intensity of the absorbance of light, which was then read in an ELISA plate reader at 570 nm.

Table 1
Crystal data and structure refinement for **1**–**3**.

	1	**2**	**3**
Empirical formula	$C_{18}H_{20}FN_5S$	$C_{36}H_{38}F_2N_{10}S_2Zn$	$C_{40}H_{44}F_2N_{10}O_4S_2Zn_2$
Formula weight	357.45	778.25	961.71
Temperature (K)	100(2)	100(2)	100(2)
Wavelength (Å)	0.71073	0.71073	0.71073
Space group	Monoclinic, P 21/c	Monoclinic, P 21/c	Monoclinic, P 21/c
Unit cell dimensions	0.31 × 0.13 × 0.09	0.35 × 0.12 × 0.06	0.48 × 0.35 × 0.04
a (Å)	18.0664(10)	9.3680(6)	9.8053(5)
b (Å)	12.0592(6)	33.020(2)	28.0511(12)
c (Å)	7.8641(5)	11.6627(7)	15.6225(9)
β (°)	95.90	107.448(2)	102.903(2)
V (Å^3)	1705.10(17)	3441.6(4)	4188.5(4)
Z, Dcalcd (Mg m^{-3})	4, 1.392	4, 1.502	4, 1.525
μ (Mo Ka) (mm^{-1})	0.211	0.890	1.308
F(0 0 0)	752	1616	1984
θ Range (°)	1.13–26.02	1.23–26.40	1.45–26.42
Reflections collected/unique	33408/3347 [*R*(int) = 0.0468]	24055/7063 [*R*(int) = 0.0354]	48308/8607 [*R*(int) = 0.0392]
Absorption correct.	Empirical	Empirical	Empirical
Range of *h*, *k*, *l*	$-22 \leqslant h \leqslant 22$, $0 \leqslant k \leqslant 14$, $0 \leqslant l \leqslant 9$	$-11 \leqslant h \leqslant 11$, $0 \leqslant k \leqslant 41$,$0 \leqslant l \leqslant 14$	$-11 \leqslant h \leqslant 12$, $0 \leqslant k \leqslant 34$,$19 \leqslant l \leqslant 0$
Refinement method	Full-matrix least-sq. on F^2	Full-matrix least-sq. on F^2	Full-matrix least-sq. on F^2
Data/restraints/param.	3347/0/226	7063/0/460	8607/0/541
Goodness-of-fit	1.040	1.008	1.015
Final *R* indices	R_1 = 0.0322	R_1 = 0.0411	R_1 = 0.0403
[*I* > 2sigma(*I*)]	wR_2 = 0.0765	wR_2 = 0.0882	wR_2 = 0.0912
R indices (all data)	R_1 = 0.0446	R_1 = 0.0629	R_1 = 0.0645
Min. and Max. Resd.	wR_2 = 0.0833	wR_2 = 0.0969	wR_2 = 0.1017
Dens. (e/Å^3)	−0.214 and 0.215	−0.479 and 1.181	−0. 446 and 0.745

2.4.2. Morphological analysis of HeLa cells death

In order to determine the mode of HeLa cell death induced by the investigated compounds, morphological analysis by microscopic examination of acridine orange and ethidium bromide stained cells was performed. HeLa cells were seeded overnight on coverslips (5×10^4 cells) in 2 mL of complete medium, and on next day treated with investigated compounds for 24 h. Concentrations applied corresponded to double IC_{50} concentrations of investigated compounds. Afterwards, the cells were examined for morphological features of apoptosis and necrosis by fluorescence microscopy using acridine orange and ethidium bromide stains (15 μL of mixture: 3 μg/mL AO and 10 μg/mL EB).

2.4.3. Cell cycle determination

Aliquots of 5×10^5 control or cells were treated with investigated compounds for 24 h (concentrations corresponded to $2 \times IC_{50}$ values) were fixed in 70% ethanol on ice for at least 1 week and centrifuged. The pellet was treated with RNase (100 μg/mL) at 37 °C temperature for 30 min and then incubated with propidium iodide (PI) (40 μg/mL) for at least 30 min. DNA content and cell cycle distribution were analyzed using a Becton Dickinson FAC-Scan flow cytometer. Flow cytometry analysis was performed using a CellQuestR (Becton Dickinson, San Jose, CA, USA), on a minimum of 10,000 cells per sample [22].

3. Results and discussion

3.1. Chemistry

Transamination of 4-methyl-4-phenyl-3-thiosemicarbazide in the presence of 1-(4-fluorophenyl)-piperazine and 2-acetylpyridine gives the ligand HAcPipPheF, **1**. The Zn(II) complexes **2** and **3** were prepared by refluxing $ZnCl_2$ or $[Zn(CH_3COO)_2(H_2O)_2]$ with the **1** in EtOH solution in a molar ratio metal (Zn(II)) to ligand of 1:2 and 1:1 respectively. The apparent pH value was adjusted to 8. The formula of compounds **1–3** was confirmed by elemental analysis, spectroscopic studies and X-ray diffraction analysis.

3.2. Spectroscopy

3.2.1. Mass spectra

The mass spectra of the soluble compounds **1–3** were recorded in MeOH solution. The ligand shows a peak at *m*/*z* 358 amu due to the parent ion fragment $[HacPyPipF+H]^+$ and at 380and 326 amu, due to the fragments $[HacPyPipF+Na]^+$ and $[HacPyPipF-S]^+$ respectively. The monomer zinc(II) complex **2** shows peak at 779 amu due to $[\mathbf{2}+H]^+$ and the dimer complex **3** shows peak at 957 amu due to $[\mathbf{3}+H]^+$. Each spectrum is associated with daughter peaks due to fragmentation.

3.2.2. Infrared spectroscopy

The significant IR bands of zinc(II) complexes are close in energy to those found in other compounds with tridentate coordination [23,24]. Coordination of the azomethine nitrogen to zinc(II) is suggested by the shift of the ν(C=N) band to lower frequencies along with the occurrence of the ν(N–N) band to higher frequency and the appearance of the band assignable to Zn–N. The thioamide band, which contains considerable ν(CS) character is found at a lower frequency, suggesting coordination of the metal through sulphur. The breathing motion of the pyridine ring is shifted to a higher frequency upon complexation and is consistent with pyridine ring nitrogen coordination. Two bands are assigned to ν(Zn–N), ν(Zn–S) and ν(Zn–N_{pyr}) for **2** indicating non-linear N–Zn–N, S–Zn–S and N_{pyr}–Zn–$N_{pyr,}$ moieties. The ν_{as}(COO) band appears at 1654 and 1580 and ν_{sym}(COO) at 1367 and 1455 cm^{-1} for **3**. The difference, [ν_{as}(COO)–ν_{sym}(COO)] between these frequencies for **3** (287 and 135 cm^{-1}) is close to that found for anisobidentate chelate and bridging acetate mode. This is totally consistent with the X-ray structure of **3**. The Zn(II) donor atom stretching frequencies are as follows: ν(Zn–N_{imine}), 420–430; ν(Zn-S), 380–370; ν(Zn–N_{pyr}), 255–240 and Zn–O, 375–330 cm^{-1}.

3.2.3. NMR spectra

Peak assignments were based on ^{2}D NMR data {proton–proton correlated spectroscopy (^{1}H–^{1}H COSY), proton–carbon heteronuclear single-quantum coherence (^{1}H–^{13}C HSQC) and proton–carbon heteronuclear multiple-bond correlation (^{1}H–^{13}C HMBC)}. In the ^{1}H and ^{13}C NMR spectra of the Zn(II) complexes **2** and **3** the hydrogen and carbon atoms of the pyridyl ring were shifted upon coordination, which indicated variations in the electron density of the pyridyl ring. The C=S resonance of the thiosemicarbazone moiety in **1** resonated at 184.37 ppm, in the complexes **2** and **3**, upfield shifts were observed, indicating increased electron density at this site on complexation and due probably to back π-bonding for thiolato sulphur [11].

3.3. Crystal structures

Selected interatomic distances and bond angles are collected in Table 2. Compounds **1**–**3** were recrystallized from $CHCl_3$/hexane, $CHCl_3$/THF and $CHCl_3$/hexane, to furnish yellow prisms suitable for single-crystal X-ray analysis.

3.3.1. Crystal structure of HAcPipPheF

Fig. 1a shows a perspective view of the HAcPipPheF molecule with the numbering scheme. HAcPipPheF is the bifurcated E′ conformation similar to that found in 2-acetylpyridine 3-hexamethyleneiminylthiosemicarbazone, HAchexim [25] and 2-pyridineformamide hexamethyleneiminylthiosemicarbazone, HAmhexim [26]. The thiosemicarbazone moiety shows an E configuration about the bonds C(16)–N(12), N(12)–N(13) and Z configuration about the bond C(17)–N(13). The thiosemicarbazone moiety is almost planar except for the sulphur atom, that presents a deviation from planarity, of the order of 0.253(1) Å. The bond distance C(17)–S(1) is formally a single bond in **1** has a length of 1.712(2) Å, Scheme 1. The bond distances and angles for **1** are similar to those reported for the bifurcated HAchexim [25] and HAmhexim [26]. The bond distance C(17)–S(1) has a length of 1.70(1) Å in HAchexim [25] and 1.732(4) in HAmhexim [26] and is formally a single bond, but in 2-hydroxy-4-methoxyacetophenone *N*4-dimethyl thiosemicarbazone is 1.65(2) Å and is formally a double bond [27]. The C(16)–N(12)–N(13) angle is 124.16(13)° for **1**, 125(1)° for HAchexim [25] and 122.8(3)° for HAmhexim [26]. The azomethine C(16)–N(12) bond is a double bond, while the N(12)–N(13) and both thioamide C(17)–N(13) and C(17)–N(14) bond distances exhibit partial double-bond character. This is indicative of a greater conjugation and an extensive delocalized electron density on the thiosemicarbazone backbone. The dihedral angle between the mean planes of the N4-1-(4-fluorophenyl) and the piperazinyl ring is 32.44(7)°.

The monomers of **1** form hydrogen-bonded dimer linked by two weak C(12)–H(12)···S(1) hydrogen bonds involving the carbon C(12)–H(12) hydrogen atom and the sulphur S(1) and vice versa of centrocymmetrically related pairs of molecules. The observed hydrogen-bonding pattern is of the DA = DA type. Intra and intermolecular hydrogen bonds stabilize the structure, while the crystal packing is determined by π–π interactions. The most significant π–π interaction is that between the pair of pyridyl rings at a centre-to-centre separation of 3.9340(9) Å, Fig. 1b.

Table 2
Selected bond lengths (Å) and angles (°) for **1**–**3**.

1		**2**		**3**	
S(1)–C(17)	1.712(2)	Zn(1)–N(12)	2.114(2)	Zn(1)–O(21)	2.041(2)
F(1)–C(23)	1.363(2)	Zn(1)–N(32)	2.138(2)	Zn(1)–O(11)	2.048(2)
N(11)–C(11)	1.334(2)	Zn(1)–N(31)	2.221(2)	Zn(1)–N(12)	2.084(2)
N(11)–C(15)	1.352(2)	Zn(1)–N(11)	2.252(2)	Zn(1)–N(11)	2.133(2)
N(12)–C(16)	1.297(2)	Zn(1)–S(2)	2.4271(7)	Zn(1)–S(1)	2.3566(8)
N(12)–N(13)	1.355(2)	Zn(1)–S(1)	2.4545(8)	Zn(1)–Zn(2)	3.5529(5)
N(13)–C(17)	1.347(2)	S(1)–C(17)	1.742(3)	Zn(2)–O(12)	2.000(2)
N(14)–C(17)	1.364(2)	S(2)–C(37)	1.732(3)	Zn(2)–O(21)	2.052(2)
N(14)–C(27)	1.462(2)	F(1)–C(23)	1.360(3)	Zn(2)–N(32)	2.113(2)
N(14)–C(18)	1.463(3)	F(2)–C(43)	1.368(3)	Zn(2)–N(31)	2.126(2)
N(15)–C(20)	1.426(2)	N(12)–C(16)	1.291(3)	Zn(1)–O(22)	2.696(2)
N(15)–C(19)	1.462(2)		1.294(3)	S(1)–C(17)	1.742(3)
N(15)–C(26)	1.469(2)	N(32)–C(36)		S(2)–C(37)	1.751(3)
C(11)–N(11)–C(15)	117.41(13)	N(12)–Zn(1)–N(32)	159.46(8)	O(21)–Zn(1)–O(11)	99.39(8)
C(16)–N(12)–N(13)	124.16(13)	N(12)–Zn(1)–N(31)	91.90(8)	O(21)–Zn(1)–N(12)	141.87(9)
C(17)–N(13)–N(12)	111.21(12)	N(32)–Zn(1)–N(31)	74.26(8)	O(11)–Zn(1)–N(12)	117.50(9)
C(17)–N(14)–C(27)	121.61(12)	N(12)–Zn(1)–N(11)	74.33(8)	O(21)–Zn(1)–N(11)	96.15(8)
C(17)–N(14)–C(18)	121.93(12)	N(32)–Zn(1)–N(11)	90.05(8)	O(11)–Zn(1)–N(11)	88.72(9)
C(27)–N(14)–C(18)	112.67(11)	N(31)–Zn(1)–N(11)	89.08(8)	N(12)–Zn(1)–N(11)	76.46(9)
C(20)–N(15)–C(19)	115.50(12)	N(12)–Zn(1)–S(2)	112.98(6)	O(21)–Zn(1)–S(1)	103.65(6)
C(20)–N(15)–C(26)	114.03(11)	N(32)–Zn(1)–S(2)	79.65(6)	O(11)–Zn(1)–S(1)	98.12(7)
C(19)–N(15)–C(26)	110.26(11)	N(31)–Zn(1)–S(2)	153.90(6)	N(12)–Zn(1)–S(1)	81.50(6)
N(11)–C(11)–C(12)	123.84(14)	N(11)–Zn(1)–S(2)	90.20(6)	N(11)–Zn(1)–S(1)	157.62(7)
		N(12)–Zn(1)–S(1)	79.90(6)	O(12)–Zn(2)–O(21)	100.32(8)
		N(32)–Zn(1)–S(1)	115.40(6)	O(12)–Zn(2)–N(32)	108.13(9)
		N(31)–Zn(1)–S(1)	93.52(6)	O(21)–Zn(2)–N(32)	150.42(8)
		N(11)–Zn(1)–S(1)	154.17(6)	O(12)–Zn(2)–N(31)	97.58(9)
		S(2)–Zn(1)–S(1)	98.35(3)	O(21)–Zn(2)–N(31)	92.78(8)
				N(32)–Zn(2)–N(31)	75.86(9)
				O(12)–Zn(2)–S(2)	110.39(6)
				O(21)–Zn(2)–S(2)	97.10(6)
				N(32)–Zn(2)–S(2)	80.71(6)
				N(31)–Zn(2)–S(2)	147.97(6)
				Zn(1)–O(21)–Zn(2)	120.46(10)

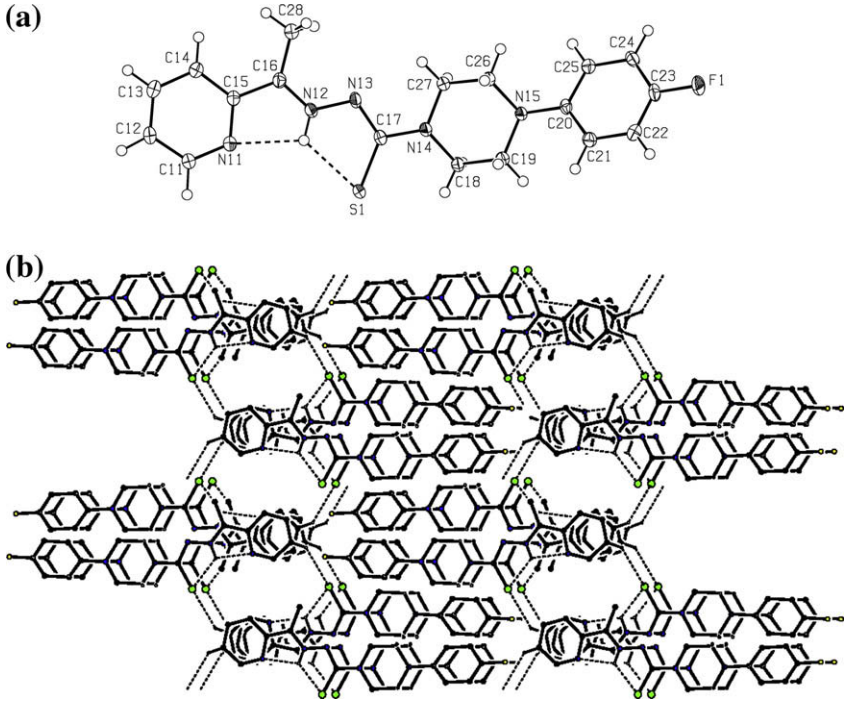

Fig. 1. (a) Labelled ORTEP diagram of **1** with 50% thermal probability ellipsoids and (b) packing diagram of **1** and along the *c* axis.

3.3.2. Crystal structure of [Zn(AcPipPheF)$_2$]

A perspective view of the centrosymmetric structure of [Zn(AcPipPheF)$_2$] is shown in Fig. 2. The two anionic AcPipPheF ligands act as tridentates which coordinate to zinc(II) through the pyridyl nitrogen, N(11) and N(31), the azomethine nitrogen, N(12) and N(32) and the thiolato sulphur atoms. The tridentate li-

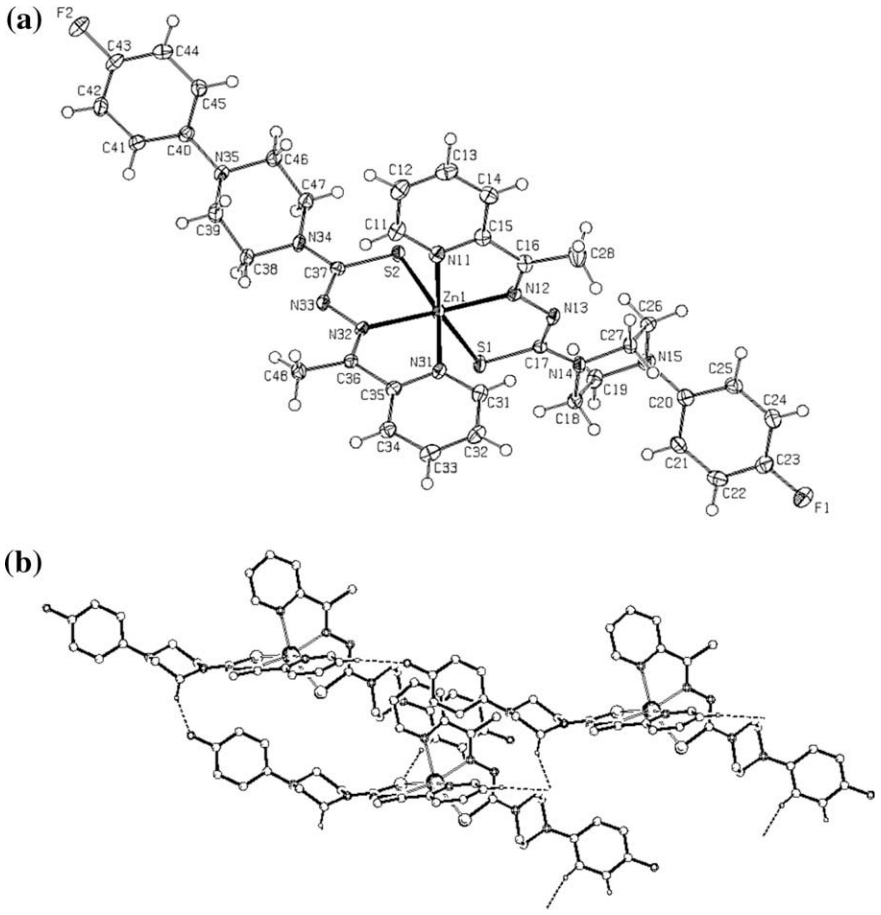

Fig. 2. (a) Labelled ORTEP diagram of **2** with 40% thermal probability ellipsoids and (b) hydrogen-bonding pattern of **2**.

gands have a ZEZ configuration based on the C(15)–C(16), N(13)–C(17), N(14)–C(17) and C(35)–C(36), N(33)–C(37), N(34)–C(37) bonds for the two ligands respectively. The zinc(II) metal ion is coordinated in a distorted octahedral configuration in a *trans*-N(12)N(32)-*cis*-N(11)N(31)-*cis*-S configuration. The *trans* angle involving the two imine nitrogens, N(12)–Zn–N(32), is 159.46(8)° is far from 180°. The N(11)–Zn(1)–N(31) angle is 89.08(8)°, while the S(1)–Zn–S(2) angle is 98.35(3)° and demonstrate that the two ligands exert significant steric effects on each other. The smallest *cis* bond angles about the Zinc centre occur for donor atoms in the same ligand {e.g. N(32)–Zn–N(31), 74.26(8)° and N(12)–Zn–N(11) 74.33(8)°}. AcPipPheF ligands have essentially equivalent Zn–S, Zn–N(imine) and Zn–N(pyridine) bond distances.

Coordination lengthens the thiosemicarbazone moiety's C(17)–S(1) and C(37)–S(2) bonds from 1.712(2) Å in HAcPipPheF to 1.742(3) and 1.732(3) Å respectively. The bond length S–C indicates an increased single-bond character and both thioamide bond distances indicate increased double-bond character and suggest a charge delocalization in the thiosemicarbazone moiety. The ligands are not planar, as indicated by the dihedral angle between the mean planes of the pyridyl ring and the chelate ring Zn–S–C–N–N, with values of 12.40(11) and 6.64(10) for the two ligands respectively. The two chelated rings are planar, as indicated by the dihedral angle between the mean planes of the Zn–S–C–N–N and the Zn–N–C–C–N, with values of 2.62(9)° and 1.37(3)° for the two ligands respectively. The dihedral angle between the mean planes of the N4-1-(4-fluorophenyl) and the piperazinyl ring is 67.34(14)° and 49.63(14)° for the two ligands respectively. C–H···S and C–H···F2 intermolecular bond connect the monomers of **2**. Intra and intermolecular hydrogen bonds stabilize the structure, while the crystal packing is determined by π–π interactions, Table 3. A double π–π interaction occurs between the pyridyl ring and the N4-1-(4-fluorophenyl) ring (symmetry operation; $1+x, y, 1+z$; $-1+x, y, -1+z$) at a centre-to-centre separation of 3.788(2) and 3.778(2) Å respectively.

3.3.3. Crystal structure of [Zn(AcPipPheF)(OAc)]$_2$

The Zn(II) ions are linked by two acetato groups. One of them bridges in the classical $\eta^1{:}\eta^1{:}\mu_2$ fashion with Zn(2)–O(12) and Zn(1)–O(11) distances of 2.000(2) and 2.048(2) respectively and the other one bridges in the less common $\eta^2{:}\eta^1{:}\mu_2$ fashion; this latter has an oxygen atom O(22) bound terminally to one Zn atom, and the other oxygen atom O(21) bound in a μ_2 bridging manner to both Zn atoms, forming a monoatomic bridge with Zn(1)–O(21) and Zn(2)–O(21) distances of 2.041(2) and 2.052(2) Å respectively. The Zn(2) atom is, however, subjected to a sixth weaker interaction in the form of a carboxylato oxygen atom, O(22), approaching the Zn(2) atom. The distance Zn(2)···O(22) 2.696(2) Å is considered as a weak bond distance. One terminal *AcPipPheF* monoanion at each metal ion complete a five and six – coordination for Zn(2) and Zn(1) metal ions respectively, Fig. 3. The zinc metal centres are connected by two inequivalent bridging acetate ligands to give a Zn···Zn distance of 3.5529(5) Å. A similar dimer structure was found for [Zn(Amhexim)(OAc))]$_2$ where Amhexim represents the anion of 2-pyridineformamide3Hexamethyleneiminylthiosemicarbazone [26].

The two anionic AcPipPheF ligands act as tridentates which coordinate to zinc(II) through the pyridyl nitrogen, N(11) and N(31), the azomethine nitrogen, N(12) and N(32) and the thiolato sulphur atoms. The tridentate ligands have a ZEZ configuration

Table 3
Inter- and intra-molecular hydrogen bonds and π–π intermolecular interactions.

1[a]		Cg–Cg[b]	β[c]	CgI–Perp[d]	CgJ–Perp[e]
Cg(1)–> Cg(1)^{i}		3.9340(9)	24.67	3.5751(6)	−3.5406(6)
Cg(1)–> Cg(1)^{ii}		3.9341(9)	25.84	−3.5407(6)	3.5751(6)
D	H	A	D···A	H···A	⟨D – H···A
C(12)	H(12)	S(1)^{iii}	3.6565(16)	2.84	143
N(12)	H(12A)	S(1)	2.8199(13)	2.26	119
N(12)	H(12A)	N(11)	2.6287(18)	2.22	106
2[a]					
Cg(10)–>Cg(5)^{iv}		3.788(2)	28.93	−3.5721(12)	3.3155(12)
Cg(5)–> Cg(10)^{v}		3.778(2)	19.44	3.3155(12)	−3.5721(12)
D	H	A	D···A	H···A	⟨D–H···A
C(21)^{vi}	H(21)	S(2)	3.595(3)	2.85	138
C(32)^{vii}	H(32)	F(2)	3.323(3)	2.46	153
C(38)^{vi}	H(38A)	F(2)	3.264(4)	2.38	149
C(18)	H(18B)	S(1)	3.071(3)	2.53	114
C(47)	H(47A)	S(2)	3.032(3)	2.55	115
C(38)	H(38B)	N(33)	2.704(4)	2.26	107
C(48)	H(48B)	N(33)	2.752(4)	2.37	104
C(27)	H(27B)	N(13)	2.698(4)	2.25	109
3[a]					
Cg(5)–> Cg(7)^{viii}		4.0115(15)	29.36	−3.2346(10)	3.4961(11)
Cg(7)–> Cg(5)^{vi}		4.0115(15)	36.26	3.4961(11)	−3.2347(10)
Cg(9)–> Cg(7)^{viii}		3.744(2)	26.41	−3.3241(11)	3.3534(11)
D	H	A	D···A	H···A	⟨D–H···A
C(2)^{ix}	H(2C)	F(2)	3.340(4)	2.53	140
C(13)^{vi}	H(13)	O(12)	3.184(4)	2.43	134
C(24)^{x}	H(24)	S(1)	3.725(3)	2.82	163
C(32)^{xi}	H(32)	O(22)	3.326(4)	2.56	140
C(33)^{viii}	H(33)	O(22)	3.087(4)	2.41	129
C(18)	H(18B)	S (1)	2.948(3)	2.46	109
C(28)	H(28C)	N(13)	2.768(4)	2.36	104
C(38)	H(38B)	S(2)	2.971(3)	2.50	110
C(48)	H(48B)	N(33)	2.825(4)	2.40	106

D, Donor; A, Acceptor.
[a] Where Cg(1) is referred to the centroid N11–C11–C12–C13–C14–C15 for 1; Cg(5) and Cg(10) are referred to the centroids N11–C11–C12–C13–C14–C15 and C40–C41–C42–C43–C44–C45 respectively for 2; Cg(5), Cg(7) and Cg(9) are referred to the centroids Zn2N32C36C35N31, N11–C11–C12–C13–C14–C15 and N31–C31–C32–C33–C34–C35 for 3.
[b] Cg–Cg is the distance between ring centroids; symmetry transformations, (i)= *x*, 3/2 − *y*, −1/2 + *z*; (ii) *x*, 3/2 − *y*, 1/2 + *z*; (iii) −*x*, 1 − *y*, 1 − *z*; (iv) 1 + *x*, *y*,1 + *z*; (v) −1 + *x*, *y*, −1 + *z*; (vi) −1 + *x*, *y*, *z*; (vii) −2 + *x*, *y*, −1 + *z*; (viii) 1 + *x*, *y*, *z*; (ix) 1 − *x*, 1/2 + *y*, −5/2 − *z*; *x*, *x*,1/2 − *y*, 1/2 + *z*; (xi) −*x*, −*y*, −1 − *z*.
[c] Where β is the angle Cg(I)–>Cg(J) or Cg(I)–>Me vector and normal to plane I (°).
[d] CgI–Perp is the perpendicular distance of Cg(I) on ring J.
[e] CgJ–Perp is the perpendicular distance of Cg(J) on ring I.

based on the C(15)–C(16), N(13)–C(17), N(14)–C(17) and C(35)–C(36), N(33)–C(37), N(34)–C(37) bonds for the two ligands respectively.

Analysis of the shape determining angles for Zn(2), using the approach of Reedijk and co-workers [28], yields a $\tau = (\alpha - \beta)/60$) {(150.42 − 147.97)/60 = 0.04) value of 0.04 for Zn(2), (τ = 0.0 and 1.0 for *SP* and *TBP* geometries respectively). The metal coordination geometry is therefore described as distorted square pyramidal with the O(12) atom occupying the apical position. The donor O(12) atom is chosen as apex by the simple criterion that it should not be one of the oxygen atoms which define either of the two largest L–Zn–L angles, α and β and the atoms N(31), N(32), S(2) and O(21) define the planar plane (maximum deviation 0.006(2) Å). The Zn(2) atom is 0.5205(3) Å out of the basal plane. The Zn(1) metal ion is coordinated in a distorted octahedral configuration. The ligands are not planar, as indicated by the dihedral angle between the mean planes of the pyridyl ring and the chelate ring Zn–S–C–N–N, with values of 8.89(11)° and 14.08(11)° for the two ligands respectively. The dihedral angle between the mean planes of the six-membered ring Zn(1)–O(11)–C(2)–O(12)–Zn(2)–O(21) and the five-membered ring Zn–N–C–C–N is 89.39(9)° and 80.95(9)° for the two ligands respectively. The dihedral angle between the mean planes of the N4-1-(4-fluorophenyl) and the piperazinyl ring is 39.55(11)° and 33.30(14)° for the two ligands respectively. C–H···S and C–H···F(2) intermolecular hydrogen bonds connect the monomers of **3**. Also, the terminal oxygen O(22) forms two C–H···O(22) intermolecular hydrogen bonds. Intra and intermolecular hydrogen bonds stabilize the structure, while the crystal packing is determined by π–π interactions, Table 3. The most significant π–π interaction is that between the pyridyl rings at a centre-to-centre separation of 3.744(2) Å.

3.4. Biological evaluation

3.4.1. In vitro antiproliferative activity

The results of cytotoxic activity *in vitro* are expressed as IC_{50} – the concentration of compound (in M) that inhibits a proliferation rate of the tumor cells by 50% as compared to control untreated cells. The compounds **1–3** were tested for their antiproliferative activity *in vitro* against the cells of four human cancer cell lines: HeLa (cervix adenocarcinoma cell line), K562 (chronic myelogenous leukaemia), MDA-MB-361 and MDA-MB-453 (breast cancer cell lines). The antiproliferative activity of compounds is presented in Table 3 along with the activity of *cis*-platin and $ZnCl_2$. Results showed that the ligand as well as the complexes demonstrated excellent antiproliferative activity, IC_{50} values range from 26 to 90 nM, against all cell lines tested, while for *cis*-platin the IC_{50} values range from 2 to 17 μM and for the zinc salt, $ZnCl_2$, the IC_{50} val-

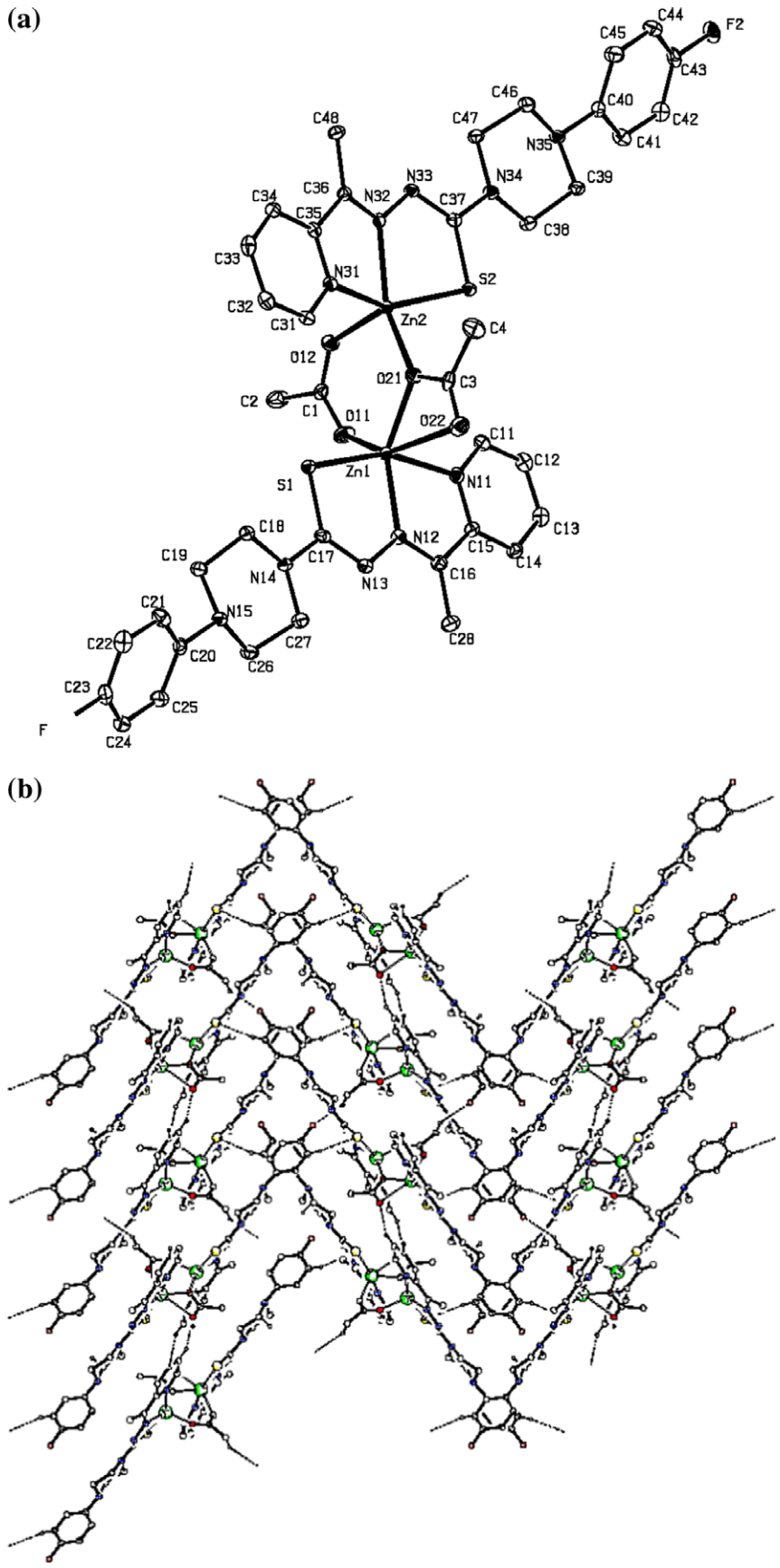

Fig. 3. (a) Labelled ORTEP diagram of **3** with 40% thermal probability ellipsoids and (b) packing diagram of **3** along the *a* axis.

Table 4
IC_{50} (M) values of the studied compounds.

Compounds	HeLa	MDA-MB-361	MDA-MB-453	K562
1	$58 \pm 8 \times 10^{-9}$	$90 \pm 2 \times 10^{-9}$	$59 \pm 5 \times 10^{-9}$	$26 \pm 6 \times 10^{-9}$
2	$55 \pm 2 \times 10^{-9}$	$56 \pm 15 \times 10^{-9}$	$61 \pm 9 \times 10^{-9}$	$71 \pm 2 \times 10^{-9}$
3	$\mathbf{35 \pm 2 \times 10^{-9}}$	$\mathbf{42 \pm 9 \times 10^{-9}}$	$\mathbf{30 \pm 2 \times 10^{-9}}$	$\mathbf{25.5 \pm 6 \times 10^{-9}}$
Cis-platin	$2.1 \pm 0.2 \times 10^{-6}$	$17.1 \pm 1.2 \times 10^{-6}$	$3.6 \pm 0.5 \times 10^{-6}$	$7.9 \pm 0.2 \times 10^{-6}$
$ZnCl_2$	$85.4 \pm 0.2 \times 10^{-6}$	$91.4 \pm 0.5 \times 10^{-6}$	$93.0 \pm 0.2 \times 10^{-6}$	$81.9 \pm 0.7 \times 10^{-6}$

Concentrations of examined compounds that induced a 50% decrease in HeLa, MDA-MB-361, MDA-MB-453, and K562 cell survival (expressed as IC_{50} (M)) the compounds were incubated with cells for 72 h. At the end of this incubation period, antiproliferative activity *in vitro* was determined by the MTT assay. Results are presented as the mean value ± SD of three independent experiments.

ues range from 81 to 93 μM. The $ZnCl_2$ exhibits poor cytotoxic activity in all these four lines (see Table 4).

Platinum(II) complexes of N4-ethyl 2-formyl and 2-acetylpyridine thiosemicarbazones showed cytotoxicity and were found to be able to overcome the *cis*-platin resistance of A2780/Cp8 cells [13]. Pt(II) or Pd(II) complexes with N4-ethyl 2-acetylpyridine thiosemicarbazone were tested in a panel of human tumor cell lines of different origins (breast, colon, and ovary cancers), and *cis*-platin-refractory/resistant cell lines and were found to exhibit very remarkable growth inhibitory activities with mean IC_{50} values of 0.9–0.5 nM and support the hypothesis that both $[Pt(Ac4Et)_2]$ and $[Pd(Ac4Et)_2]$ complexes can be characterized by cellular pharmacological properties distinctly different from those of *cis*-platin [29]. The complexes $[ZnCl_2(Fo4Npypipe)]$ and $[ZnCl_2(Ac4Npypipe)]$ where Fo4Npypipe and Ac4Npypipe are the monoion of 2-formyl pyridine N(4)-1-(2-pyridyl)-piperazinyl thiosemicarbazone and 2-acetyl pyridine N(4)-1-(2-pyridyl)-piperazinyl thiosemicarbazone have been evaluated *in vitro* against MCF-7, T24, A-549 and L-929 cell lines and it was found to exhibit remarkable antiproliferative activity with mean IC_{50} values of 0.2–20 μM [11].

The IC_{50} values for **1** against MDA-MB-361 and MDA-MB-453 cell lines are 90 and 59 nM respectively and against HeLa and K562 cell lines are 59 and 26 nM respectively. Ligand **1** is **190** and 61 times more active than *cis*-platin against MDA-MB-361 and MDA-MB-453 and 36 and **303** times more active than *cis*-platin against HeLa and K562 cell lines. The IC_{50} values for **2** against MDA-MB-361 and MDA-MB-453 cell lines are 56 and 61 nM respectively and against HeLa and K562 cell lines are 55 and 71 nM respectively. The Zn(II) complex **2** is **305** and 59 times more active than *cis*-platin against MDA-MB-361 and MDA-MB-453 and 38 and **111** times more active than *cis*-platin against and K562 cell lines. In the case of HeLa and MDA-MB-453 cell lines the ligand and complex **2**, the IC_{50} values are in the same nM range 30–38 times for the former and 60 times for the latter cell line more cytotoxic compared to *cis*-platin. In this case the observed cytotoxicity is probably due to the cytotoxicity of the ligand and the metal complexes may be a vehicle for activation of the ligand as the cytotoxic agent. Ligand **1** and complex **2** exhibited high activity as anticancer agent against all four cancer cell lines, and **1** exhibits the highest selectivity against K562.

The IC_{50} values for **3** against MDA-MB-361 and MDA-MB-453 cell lines are 42 and 30 nM respectively and against HeLa and K562 cell lines are 35 and 26.5 nM respectively. The Zn(II) complex **3** is **406** and 120 times more active than *cis*-platin against MDA-MB-361 and MDA-MB-453 and 60 and **298** times more active than *cis*-platin against HeLa and K562 cell lines. The most outstanding results are obtained from the activity of compound **3**, which is 60–405 times better tha *cis*-platin. According to these results, **3** is the most active compound of this study. It is noteworthy the high selectivity against MDA-MB-453 and K562 cancer cell lines.

The mentioned evident differences in the antiproliferative action of the ligand and its zinc(II) complexes indicate that the zinc(II) complexes really exist under the condition of the biological tests. Interestingly enough, **1–3** were found to be more potent cytotoxic agent than the prevalent benchmark metallodrug, *cis*-platin, under the same experimental conditions measured by us. The superior activity of **1–3** assumes significance in light of the fact that *cis*-platin is undisputedly the most studied and widely used metallopharmaceutical for cancer therapy known to date.

3.4.2. Fluorescence microscopy

Compounds **1–3** at a concentration of $2 \times IC_{50}$ nM, after a 24 h continuous action, effectively induce cell apoptosis, rounding and detachment in HeLa cells. In addition to their growth inhibition activities, marked cytopathological effects, spherical morphology and detachment of the cells, were observed on the HeLa cells treated with the compounds.

3.4.3. Cell cycle analysis

Flow cytometry was used to determine the effects of compounds **1–3** on the cell cycle phase distribution of each of the tumor cell lines. The effect of compounds upon the cell cycle was assessed after incubating cells with the compounds at their $2 \times IC_{50}$ nM. Incubation of the K562, HeLa and MDA-MB-453 cells with **1–3** led to accumulation of more cells in S phase and a reduction of cell population in G2/M phase, Table 5. The S-phase cell cycle arrest observed in the cells treated with the compounds suggests that these new complexes inhibit DNA synthesis of the malignant cells. It has been reported that thiosemicarbazones

Table 5
Effect of **1–3** on cell cycle progression.[a]

	G0/G1	S	G2/M
Hela			
Control	52.52	16.17	28.15
1	51.17	30.22	13.86
2	59.32	17.44	19.92
3	57.33	23.17	14.93
K-562			
Control	49.81	21.45	19.68
1	46.6	32.86	16.31
2	48.19	35.18	12.1
3	46.36	31.98	17.09
MDA-MB-361			
Control	50.78	17.31	29.44
1	70.14	9.56	18.99
2	76.28	6.42	16.13
3	72.2	6.5	20.06
MDA-MB-453			
Control	67.11	14.27	14.93
1	55.98	22.29	14.83
2	67	15.03	12.24
3	60.83	24.07	8.21

[a] Effect of **1–3** on cell cycle phase distribution. HeLa, K562, MDA-MB-361, and MDA-MB-453 cell lines were exposed to compounds ($2 \times IC_{50}$ nM) for 24 h and then collected for analysis of cell cycle phase distribution using flow cytometry. Percentage of cells under different stages of cell cycles (G0–G1, S, G2–M) is shown.

and their derivatives inhibited cancer cell proliferation through various mechanisms, such as inhibiting ribonucleotide reductase or the RNA dependent DNA polymerase, inducing oxygen active species or reacting with cell thiols [30]. Mechanisms of S-phase cell cycle arrest by the compounds **1–3** in these malignant cells remain to be elucidated. Incubation of the cell line MDA-MB-361 with compounds **1–3** exhibits an increase in the percent of cells population in Go/G1 phase. It is known that *cis*-platin induces DNA damage and arrest the cells at the G2/M phase of the cell cycle [31].

Acknowledgments

We thank the NMR and Mass spectra service of the University of Ioannina, Greece. We thank the Ministry for Development, General Secretariat for Research and Technology of Greece for funding of a joint research and technology programme. This work was financed by Ministry of Science and Technological Development of Serbia Grant No. 145006.

Appendix A. Supplementary material

Supplementary data associated with this article can be found, in the online version, at doi:10.1016/j.jinorgbio.2009.12.021. Figs. S1–S4 exhibit HeLa cells cultured with 2 × IC50 of **1–3** under the fluorescence microscope. Crystallographic data for the structural analyses have been deposited at *Cambridge Crystallographic Data Centre*, as deposition numbers CCDC 718694, 718695 and 718696 for **1**–**3** respectively. Copies of these data may be obtained, free of charge, from CCDC, 12 Union Road, Cambridge CB2 1EZ, UK, *via* fax (+44 1223 336 033), e-mail (deposit@ccdc.cam.ac.uk), or internet (www.ccdc.cam.ac.uk).

References

[1] R.A. Finch, M.-C. Liu, S.P. Grill, W.C. Rose, R. Loomis, K.M. Vasquez, Y.-C. Cheng, A.C. Sartorelli, Biochem. Pharm. 59 (2000) 983–991. and references therein.
[2] A.E. Liberta, D.X. West, Biometals 5 (1992) 121–126.
[3] H. Beraldo, D. Gambino, Mini Rev. Med. Chem. 4 (2004) 159–165.
[4] A. Gomez Quiroga, C. Navarro Ranninger, Coord. Chem. Rev. 248 (2004) 119–133.
[5] S. Halder, S-M. Peng, G-H. Lee, T. Chatterjee, A. Mukherjee, S. Dutta, U. Sanyald, S. Bhattacharya, New J. Chem. 32 (2008) 105–114.
[6] M. Belicchi-Ferrari, F. Bisceglie, C. Casoli, S. Durot, I. Morgenstern-Badara, G. Pelosi, E. Pilotti, S. Pinelli, P. Tarasconi, J. Med. Chem. 48 (2005) 1671–1675.
[7] G.K. Walkup, S.C. Burdette, S.J. Lippard, R.Y. Tsien, J. Am. Chem. Soc. 122/23 (2000) 5644–5645.
[8] H.L. Hellmich, C.J. Frederickson, D.S. DeWitt, R. Saban, M.O. Parsley, R. Stephenson, M. Velasco, T. Uchida, M. Shimamura, D.S. Prough, Neurosci. Lett. 355/3 (2004) 221–225.
[9] J.S. Casas, M.S. García-Tasende, J. Sordo, Coord. Chem. Rev. 209 (2000) 197–261.
[10] N. Chikaraishi Kasuga, K. Sekino, M. Ishikawa, A. Honda, M. Yokoyama, S. Nakano, N. Shimada, C. Koumo, K. Nomiya, J. Inorg. Biochem. 96 (2003) 298–310.
[11] D. Kovala-Demertzi, A. Alexandratos, A. Papageorgiou, P. Nath Yadav, P. Dalezis, M.A. Demertzis, Polyhedron 27 (2008) 2731–2738.
[12] D. Kovala-Demertzi, P. Nath Yadav, J. Wiecek, S. Skoulika, T. Varadinova, M.A. Demertzis, J. Inorg. Biochem. 100/9 (2006) 1558–1567.
[13] J.P. Scovill, D.L. Klayman, C.F. Franchino, J. Med. Chem. 25 (1982) 1261–1264.
[14] Bruker, APEX2 Software, Bruker AXS Inc., V2.0-1, Madison, Wisconsin, USA, 2005.
[15] G.M. Sheldrick, SADABS, Program for Empirical Absorption Correction of Area Detector Data, University of Goettingen, Germany, 1997.
[16] G.M. Sheldrick, Acta Crystallogr. A46 (1990) 467–473.
[17] G.M. Sheldrick, SHELXL-97, Program for the Refinement of Crystal Structures, University of Goettingen, Germany, 1997.
[18] A.J.C. Wilson, International Tables for Crystallography, vol. C, Kluwer Academic Publishers, Dordrecht, The Netherlands, 1995.
[19] A.L. Spek, PLATON, A Multipurpose Crystallographic Tool, Utrecht University, Utrecht, The Netherlands, 2003.
[20] T. Mosmann, J. Immunol. Methods 65 (1983) 55–63.
[21] M. Ohno, T. Abe, J. Immunol. Methods 145 (1991) 199–203.
[22] R.H. Clothier, Methods Mol. Biol. 43 (1995) 109–118.
[23] D. Kovala-Demertzi, P. Nath Yadav, M.A. Demertzis, M. Coluccia, J. Inorg. Biochem. 78/4 (2000) 347–354.
[24] D. Kovala-Demertzi, M.A. Demertzis, J.R. Miller, C. Papadopoulou, C. Dodorou, G. Filousis, J. Inorg. Biochem. 86 (2001) 555–563.
[25] D.X. West, G.A. Bain, R.J. Butcher, J.P. Jasinski, Y. Li, R.Y. Pozdniakiv, J. Valdes-Martınez, R.A. Toscano, S. Hernandez-Ortega, Polyhedron 15 (1996) 665–674.
[26] E. Bermejo, A. Castineiras, Isabel Garcıa-Santos, D.X. West, Z. Anorg. Allg. Chem. 630 (2004) 1096–1109.
[27] D. Kovala-Demertzi, N. Kourkoumelis, M.A. Demertzis, J.R. Miller, C.S. Frampton, J.K. Swearingen, D.X. West, Eur. J. Inorg. Chem. (2000) 727–734.
[28] A. Addison, R.T. Nageswara, J. Reedijk, J. Van Rijn, G.C. Verschoor, J. Chem. Soc. Dalton Trans. (1984) 1349–1356.
[29] D. Kovala-Demertzi, A. Boccarelli, M.A. Demertzis, M. Coluccia, Chemotherapy 53 (2007) 148–152.
[30] J. Shao, B. Zhou, B. Chu, Y. Yen, Curr. Cancer Drug Targets 6 (2006) 409–431.
[31] S. Mueller, M. Schittenhelm, F. Honecker, E. Malenke, K. Lauber, S. Wesselborg, J.T. Hartmann, C. Bokemeyer, F. Mayer, Int. J. Oncol. 29 (2006) 471–479.